THE JOURNAL OF PHYSICAL CHEMISTRY C

Article

pubs.acs.org/JPCC

Nanoscale Structure of Cement: Viewpoint of Rigidity Theory

Mathieu Bauchy,*[,†,§] Mohammad Javad Abdolhosseini Qomi,[†] Christophe Bichara,[‡] Franz-Joseph Ulm,[†] and Roland J.-M. Pellenq[†,‡]

[†]Concrete Sustainability Hub, Department of Civil and Environmental Engineering, and MIT-CNRS Joint Laboratory, Massachusetts Institute of Technology, 77 Massachusetts Avenue, Cambridge, Massachusetts 02139, United States

[‡]Centre Interdisciplinaire des Nanosciences de Marseille, Aix-Marseille University, CNRS, Campus de Luminy, 13288 Marseille Cedex 09, France

[§]Department of Civil and Environmental Engineering, University of California, Los Angeles, California 90095, United States

ABSTRACT: Rigidity theory is a powerful tool to predict the properties of glasses with respect to composition. By reducing such molecular networks to simple mechanical trusses, topological constraint theory filters out all the unnecessary details that ultimately do not affect macroscopic properties. However, the usual constraint enumeration is restricted to networks that are amorphous, homogeneous, and fully connected. On the contrary, calcium−silicate−hydrate (C−S−H), the binding phase of cement, is partially crystalline and heterogeneous and shows some isolated water molecules. Here, we report how rigidity theory can be used to describe the nanoscale structure of this material by relying on molecular dynamics simulations. The distinction between intact and broken constraints is clearly defined at the atomic scale, thus allowing a precise enumeration of the topological constraints. We show that the rigidity of the C−S−H network can be increased by decreasing the Ca/Si molar ratio, which, as predicted by rigidity theory, allows improvement of the hardness of the material. This study suggests that rigidity theory could be applied with great rewards to a broader range of materials than glasses.

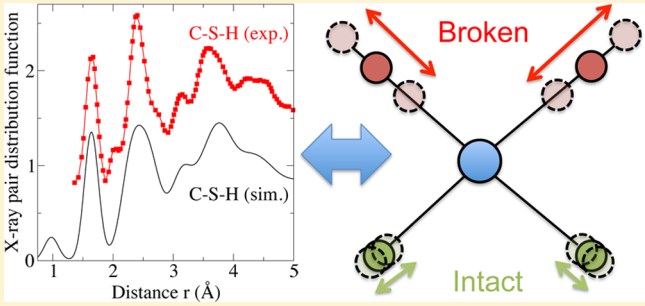

1. INTRODUCTION

Rigidity theory,[1−4] inspired by Maxwell's study on the stability of mechanical trusses,[5] has been extensively used to understand the compositional dependence of network glasses while only relying on an atomic scale analysis. A molecular network can be classified as "flexible", having internal degrees of freedom called floppy modes[6] that allow for local deformations, "stressed rigid", being locked by its high connectivity, or "isostatic", the optimal intermediate state. The isostatic state is achieved when the number of constraints per atom n_c, comprising radial bond stretching (BS) and angular bond bending (BB), equals 3, the number of degrees of freedom per atom. Compositions offering an isostatic behavior have been found to exist inside a window,[7] located between the flexible ($n_c < 3$) and the stressed-rigid ($n_c > 3$) compositions, called the Boolchand intermediate phase, and show some remarkable properties, such as a stress-free character,[8] a space-filling tendency,[9] very weak aging phenomena,[10] and anomalous behaviors, such as a fracture toughness maximum.[11]

Rigidity theory, or topological constraint theory, has been shown to be a powerful tool for predicting the mechanical properties of glass[12,13] and has been used by Corning Inc. to design the very popular Gorilla Glass 3.[14,15] This theory has also been successfully applied to proteins to study protein folding,[16,17] but it is still unclear whether it can be applied to more complex materials. In particular, the enumeration of the constraints à la Maxwell, proposed by Phillips,[1,2] assumes (a) an order limited to the short range, (b) known coordination numbers, (c) a homogeneous structure, and (d) a fully connected network.

Calcium−silicate−hydrate (C−S−H), which is the binding phase of cement,[18] does not meet any of these conditions and is, therefore, a challenging material to extend rigidity theory. Despite cement prevalence in the built environment, the molecular structure of C−S−H has just recently been proposed.[19−23] This material can be qualified as complex as, depending on its composition, (a) it shows both crystalline and amorphous features,[23] (b) the local environment of the atoms differs from that of crystals,[23] (c) it has a quasi-layered structure that is not homogeneous,[19] and (d) it shows some undissociated water molecules that are not part of the network.[24] Hence, we chose C−S−H as a base material to perform the first enumeration of the constraints in a complex material. This is achieved via a careful analysis of a realistic atomic trajectory, obtained through molecular dynamics simulations.[19,21,24]

This paper is organized as follows: The details of the model and the simulations are first presented in section 2. The

Received: March 13, 2014
Revised: May 18, 2014
Published: May 20, 2014

   dx.doi.org/10.1021/jp502550z | J. Phys. Chem. C 2014, 118, 12485−12493

algorithm allowing the enumeration of BS and BB constraints is then explained in sections 3 and 4. In section 5, we show how this approach can be used to enhance the hardness of C−S−H. Eventually, the results are discussed in section 6 and summarized in section 7.

2. NUMERICAL DETAILS

2.1. A Realistic C−S−H Model. To describe the disordered molecular structure of C−S−H, Pellenq et al.[19] proposed a realistic model for C−S−H with a stoichiometry of $(CaO)_{1.65}(SiO_2)(H_2O)_{1.73}$. We generated the C−S−H model by introducing defects in an 11 Å tobermorite[26] configuration, following a combinatorial procedure. Eleven angstrom tobermorite consists of pseudo-octahedral calcium oxide sheets, which are surrounded by silicate tetrahedral chains. The latter consists of bridging oxygen (BO) atoms and Q^2 silicon atoms (having two bridging and two nonbridging oxygen (NBO) terminal atoms).[27] These negatively charged calcium−silicate sheets are separated from each other by an interlayer spacing, which contains interlayer water molecules and charge-balancing calcium cations. Although the Ca/Si ratio in 11 Å tobermorite is 1, this ratio is increased to 1.71 in the present C−S−H model through random removal of SiO_2 groups.

The defects in the silicate chains provide possible sites for adsorption of extra water molecules. The adsorption of water molecules in the structurally defected tobermorite model was performed via the grand canonical Monte Carlo method, ensuring equilibrium with bulk water at constant volume and room temperature. The REAXFF potential,[20] a reactive potential, was then used to account for the reaction of the interlayer water with the defective calcium−silicate sheets. The use of this reactive potential allows the water molecules to dissociate into hydroxyl groups. More details on the preparation of the model and its experimental validation can be found elsewhere.[19,21,24]

2.2. Simulation Procedure. Relying on the previously presented model, we simulated a C−S−H box made of 501 atoms. We used molecular dynamics, implemented thanks to the LAMMPS package.[28] To this end, we used the REAXFF potential[20] with a time step of 0.25 fs. We first relaxed the system at zero pressure and 300 K for 2.5 ns in the NPT ensemble and made sure that convergence of the energy and volume was achieved. Subsequently, we ran a 25 ps simulation in the NVT ensemble for statistical averaging.

2.3. A Challenging Material. Figure 1 shows a snapshot of the atomic configuration of the C−S−H model. To validate the structure of the model, we computed the X-ray pair distribution function (PDF):

$$g_X(r) = \frac{1}{\sum_{i,j=1}^{n} c_i c_j b_i b_j} \sum_{i,j=1}^{n} c_i c_j b_i b_j g_{ij}(r) \quad (1)$$

where b_i is the X-ray scattering length for i atoms, which we assumed to be constant as in ref 25. Note that, to take into account the maximal scattering vector $\mathbf{Q}_{max}$ of the experimental structure factor, the computed PDFs were broadened by following the methodology described in refs 29 and 30.

Figure 2 shows the X-ray PDFs of C−S−H, compared with experimental data obtained by Monteiro et al.[25,31,32] for an artificial C−S−H specimen with Ca/Si = 1.6, fairly similar to the present composition. The first peak, around 1.0 Å, arises from H−O correlations. H−H correlations inside water molecules are merged with the peak around 1.6 Å, which

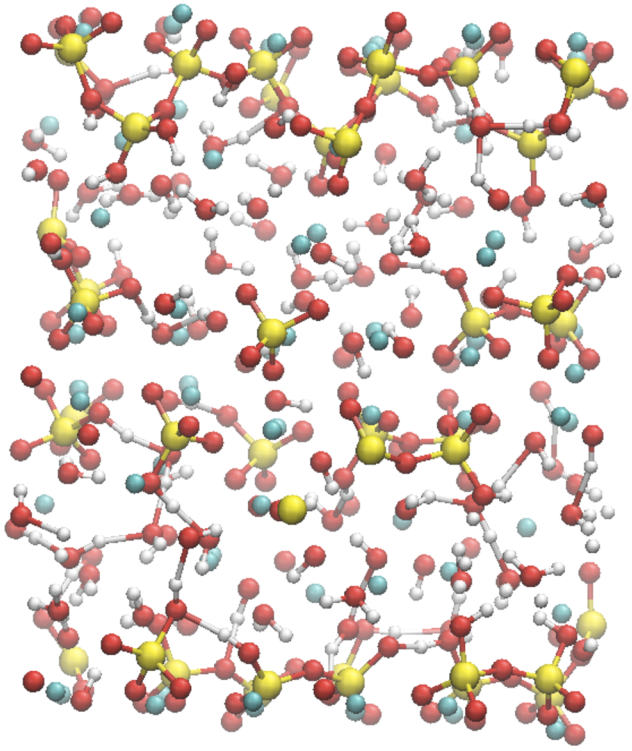

Figure 1. Snapshot of the atomic configuration of the calcium−silicate−hydrate model of composition $(CaO)_{1.71}(SiO_2)(H_2O)_{1.73}$. Silicon, oxygen, calcium, and hydrogen atoms are represented in yellow, red, cyan, and white, respectively.

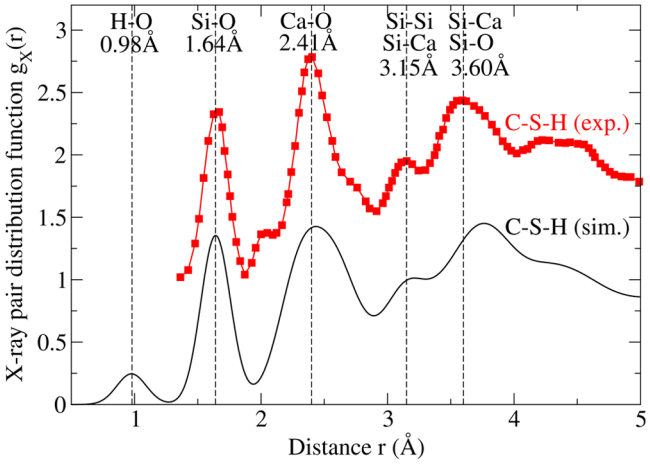

Figure 2. X-ray pair distribution function of the calcium−silicate−hydrate model, compared with experimental data for an artificial C−S−H wih Ca/Si = 1.6.[25]

corresponds to Si−O correlations around Si tetrahedra. The signification of the following peaks is less clear as they arise from a superposition of several correlations; however, Ca−O, O−O, and Si−Si correlations are, respectively, observed around 2.3, 2.7, and 3.2 Å. We note a good agreement between simulation and experiment for C−S−H, which is remarkable considering the complexity of the material. In particular, the positions and heights of the first peaks, associated with Si−O, Ca−O, and Si−Si correlations, respectively, are well reproduced by the simualtion. Although the general shape at high r is also well reproduced, we observe a slight shift of the Si−Ca peak.

dx.doi.org/10.1021/jp502550z | J. Phys. Chem. C 2014, 118, 12485−12493

Overall, the atomic structure appears to be similar to that of a silicate glass,[33] with the PDF showing broad peaks.

Although the system is globally disordered, a direct observation of the atomic configuration (see Figure 1) reveals that it maintains the layered structure characteristic of the tobermorite crystal.[22,23,26,34] This can be problematic for the enumeration of the constraints since, in crystals, some apparently intact constraints can, in fact, be mutually dependent, thus leading to an overestimation of the number of constraints. In addition, the existence of such layers means that the system is not homogeneous. For example, it has been reported that the local environment of Ca atoms inside the layers differs from that between the layers.[21,22] Therefore, the original constraint enumeration algorithm, which assumes homogeneous coordination numbers,[1] cannot be applied directly. Regarding the atomic short-range order, which directly affects the number of constraints,[1] the coordination numbers of Si, O, and H atoms are, as expected and predicted by the octet rule, respectively, 4, 2, and 1. However, similarly to Na atoms in sodium silicate glasses,[35] Ca atoms obviously do not follow the octet rule, their coordination number being, on average, between 5 and 7. This is in agreement with previous simulations of calcium silicate glasses.[36] Hence, the evaluation of the number of BS constraints created by Ca atoms is not straightforward. Eventually, despite the dissociation of some water molecules into hydroxyl groups, as allowed by the REAXFF potential, some undissociated water molecules still exist in the interlayer spacing.[24] Such molecules are not part of the network and, consequently, do not contribute to the global rigidity of the system. For all the above reasons, one needs to extend rigidity theory for application to such complex materials.

2.4. Counting the Constraints from Molecular Dynamics Simulations. One evaluates the rigidity of macroscopic mechanical trusses by enumerating the number of constraints between the nodes of the network and comparing it to the number of degrees of freedom.[5] Typically, for mechanical networks, one wants to achieve a stressed-rigid network to avoid internal degrees of freedom. The same analysis can be performed in network glasses, by enumerating BS and BB constraints, which, respectively, maintain bond lengths and angles fixed around their average value.[1,2] In homogeneous networks that are fully connected, such as Ge–Se, the enumeration of the constraints is straightforward and only depends on the coordination numbers r_i of each species. Hence, the number of BS constraints is given by $r_i/2$, since each BS constraint is shared by two atoms. On the other hand, the number of BB constraints is given by $2r_i - 3$,[1] which is the number of independent angles needed to define the polyhedron. Assuming that the system is homogeneous, one can adopt a mean-field approach, such that the average number of constraints per atom n_c is given by

$$n_c = \bar{r}/2 + 2\bar{r} - 3 \quad (2)$$

where $\bar{r}$ is the average coordination number of the atoms. The rigidity transition, or isostatic state, then occurs when $n_c = 3$, the number of constraints per atom in a three-dimensional system, which is achieved for $\bar{r} = 2.4$.

However, when the structure of the glass is not well-known, this traditional approach relies on unproven guesses about coordination numbers and whether all constraints are intact. Indeed, each constraint is associated with a given energy and can be intact or broken according to the temperature and the available thermal energy.[35,37,38] More generally, the mean-field approximation is not possible any more when the system is heterogeneous. To this end, to analyze the rigidity of C–S–H, we refined a method originally developed in ref 39 and widely applied to chalcogenide and oxide glasses since then.[35,40−48] The latter is based on the analysis of atomic trajectories obtained through molecular dynamics simulations. Since the nature of the constraints imposed on atomic motion is not known a priori, we take the opposite approach by looking at the motion of each atom and deducing the underlying constraints that cause this motion.

The basic idea of this method is summarized in Figure 3: an active constraint would maintain bond lengths or angles fixed around their average value, whereas a large atomic motion implies the absence of any underlying constraint. In more detail, to get the number of BS constraints to apply to a central atom, we observe the radial excursion of each neighbor (see Figure 3a). If a neighbor shows a small radial excursion, the existence of an underlying constraint that maintains the bond length fixed around its average value is implied. On the contrary, if the radial excursion is large, the corresponding constraint is broken. The number of BB constraints can be accessed in the same fashion by analyzing the angular excursion of each neighbor (see Figure 3b). The implementation of this method is detailed in the following sections.

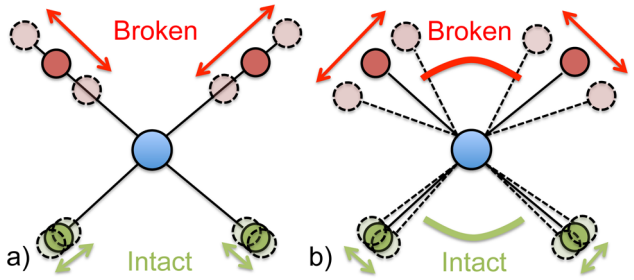

Figure 3. Method of the enumeration of (a) bond-stretching (BS) and (b) bond-bending (BB) constraints from atomic trajectories generated by molecular dynamics. Small (large) (a) radial and (b) angular excursions correspond to intact (broken) BS and BB constraints, respectively.

3. BOND-STRETCHING CONSTRAINTS

We start by computing the number of BS constraints. To evaluate the radial excursion of each neighbor around a central atom, we compute the PDFs of each pair of atoms and their decompositions into the distributions of each neighbor 1, 2, ..., 8, where the latter are identified according to their respective distances to the central atom. Here, 8 is an arbitrary number that should be large enough not to miss any constraints. An example of such decomposition is shown in Figure 4 for the Si–O PDF. The average values of these distributions correspond to the mean distances of each neighbor, which is shown in the inset of Figure 4 for Si–O as a function of the neighbor number. Here, as expected, we recover that Si atoms are 4-fold coordinated, with an average bond length of 1.6 Å. A clear jump is observed between the position of the atoms of the first coordination shell and that of the second, around 3.5 Å.

Alternatively, the second moment of these distributions, the standard deviation σ_r, gives an estimation of the radial excursion of each neighbor, i.e., the strength of the corresponding BS constraint. In other words, large σ_r values correspond to inactive constraints, whereas small ones are caused by active

dx.doi.org/10.1021/jp502550z | J. Phys. Chem. C 2014, 118, 12485−12493

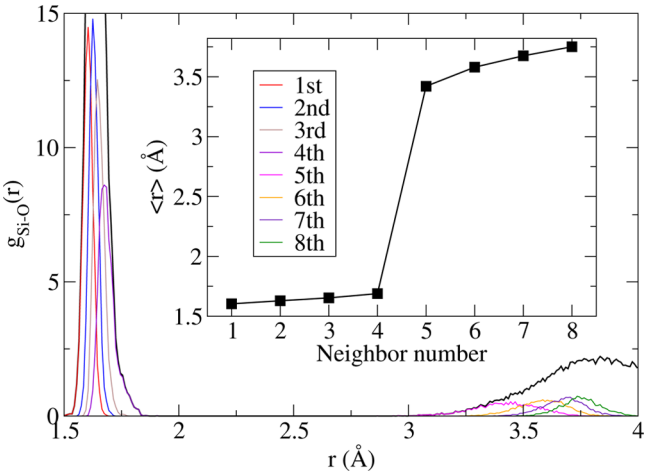

Figure 4. Si−O partial pair distribution function and its decomposition into the distributions of the eight first neighbors, out of which are computed the average distances of each neighbor, shown in the inset.

constraints. However, pairs of atoms show different bond lengths, so to allow for a consistent comparison, the standard deviations should be rescaled by the average bond length. Hence, we get an estimative value of the relative excursions of each neighbor around every species of atom. Note that this analysis is equivalent to the Lindemann criterion, according to which melting is expected to occur when the root mean vibration amplitude between pairs of atoms reaches 10% of the nearest neighbor distance.[49]

The radial standard deviations σ_r, normalized by the average bond length d, are shown in Figure 5 for each pair of atoms, with respect to the neighbor number. According to a previous study on the behavior of the constraints with temperature, the approximate limit between intact and broken constraints was found to be around σ_r/d = 7%,[35] which is fairly close to the Lindemann criterion. However, for most of the other pairs of atoms, the number of active constraints weakly depends on this limit, as there is a clear gap between intact (low σ_r) and broken (large σ_r) constraints. In the case of Si−O correlations (see Figure 5a), the four first neighbors that belong to the first coordination shell show a small relative radial excursion, around 2%. On the contrary, atoms in the second coordination shell are characterized by a much larger relative radial excursion, around 17%. As expected, this implies that each Si atom shares four BS constraints with the four oxygen atoms that define the Si tetrahedron. Note that, even if C−S−H maintains a certain degree of crystallinity within the silicate layers, we find no signature of BS constraints with neighbors outside the first coordination shell that would artificially result in some mutually dependent constraints. Therefore, this method appears able to handle partially crystalline materials.

The analysis of oxygen atoms requires greater care, as different species are characterized by different local environments. Hence, O atoms are divided into BOs, NBOs, O_w, and O_h, where O_w and O_h are the O atoms that, respectively, belong to undissociated water molecules and hydroxyl groups that are not connected to any Si atom. We do not find any other species of O atoms. NBOs are further distinguished as NBO_H and NBO_{Ca} atoms, according to the cation to which they are connected. BO atoms show only two small σ_r values with the two nearest Si atoms, whereas NBOs show one active constraint with the nearest Si atom and another one with the nearest cation Ca or H (see Figure 5b,c). Water molecules and free hydroxyl groups are not part of the atomic network and, thus, do not contribute to its rigidity. Therefore, we exclude them from the enumeration. In practice, this means that we do not take into account their internal constraints as well as the degrees of freedom of their atoms.

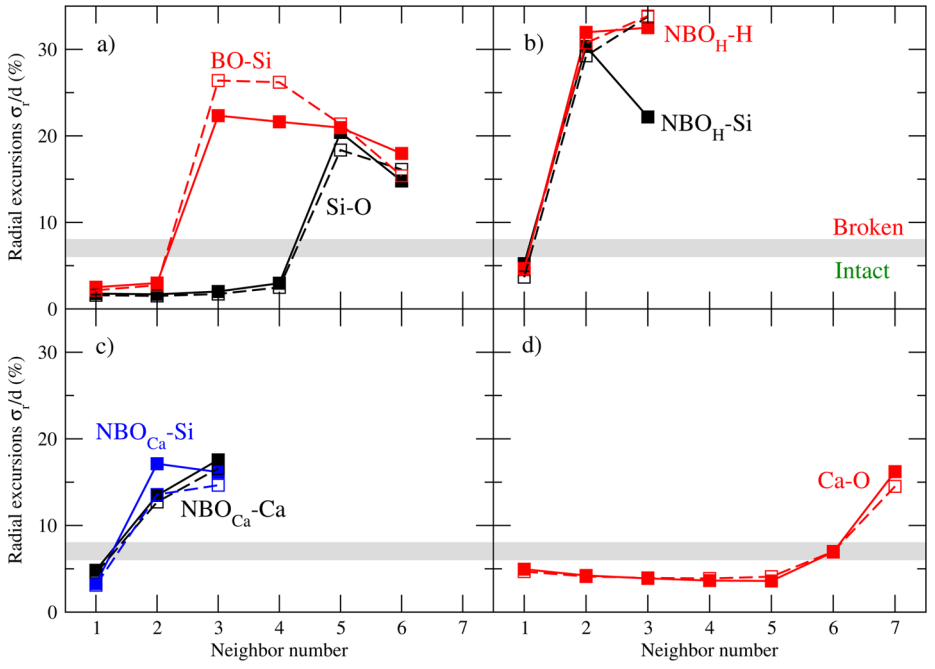

Figure 5. (a) Si−O and BO−Si, (b) NBO_H−Si and NBO_H−H, (c) NBO_{Ca}−Si and NBO_{Ca}−Ca, and (d) Ca−O radial standard deviations σ_r as a function of the neighbor number, where BO, NBO_H, and NBO_{Ca} correspond to bridging oxygen and nonbridging oxygen around H and Ca atoms, respectively. In all cases, the shaded area indicates an approximate limit between intact (low σ_r) and broken (large σ_r) bond-stretching constraints. Results for a C−S−H sample with Ca/Si = 1.09 are added for comparison (open symbols).

dx.doi.org/10.1021/jp502550z | J. Phys. Chem. C 2014, 118, 12485−12493

We note that, although the H−O, Si−O, and Ca−O bond lengths are very different (respectively, around 1.0, 1.6, and 2.3 Å), the relative radial motion of constrained neighbors is fairly comparable, between 2% and 6%. This supports the fact that all the constraints contribute with a similar weight to the global rigidity of the material. We keep in mind that a more subtle analysis would require consideration of these small differences, but it is the main advantage of rigidity theory to be able to provide interesting insights into macroscopic properties while filtering out these details.

The local environment of Ca atoms is less well-defined, as no clear gap is observed between low and large σ_r (see Figure 5d). It is not clear whether five or six constraints are active, as this strongly depends on the choice of the intact/broken limit. This arises from the fact that the coordination of Ca atoms, inside or between the layers, is not homogeneous; that is, all Ca atoms do not show the same number of BS constraints, which leads to unclear results when averaged on all atoms. To handle these heterogeneities, one cannot rely on a mean-field approach anymore.

To gain deeper insights into the distinction between intact and broken constraints, we compute the radial standard deviations σ_r of every neighbor for each atom individually. In practice, for each individual atom i, we track the distances of each neighbor with respect to time. This allows computation of individual values of σ_r according to the neighbor number for each atom, which are then normalized by the bond length d. Eventually, we get a distribution of the different σ_r/d values obtained for every atom. These distributions are shown in Figure 6 for the case of Si−O correlations for the six first

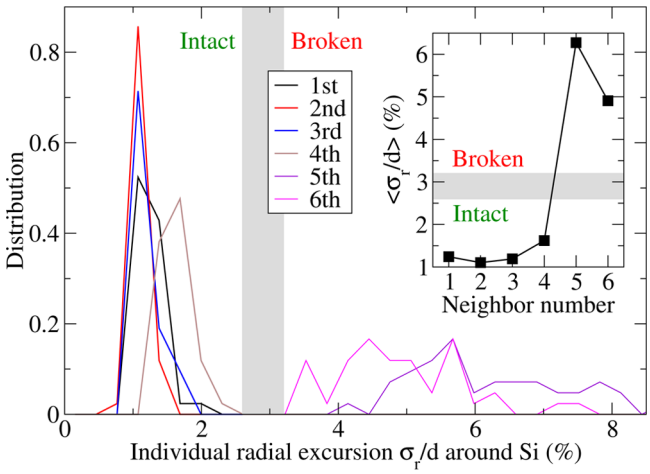

Figure 6. Distributions of the individual radial standard deviations σ_r of O atoms around Si atoms normalized by the bond length, decomposed into the contribution of each O neighbor. The inset shows the average value of each of the previous distributions with respect to the neighbor number. In both cases, the shaded area indicates an approximate limit between the intact (low σ_r) and the broken (large σ_r) bond-stretching constraints.

neighbors. We observe a clear distinction between the distributions of the four first neighbors, which are sharp and centered around low σ_r/d values, and those of the next neighbors, which are broader and centered around larger σ_r/d values. They are clearly associated with intact and broken constraints, respectively. In fact, in the case of Si−O correlations, the intact and broken σ_r/d distributions do not overlap, which allows definitino of a limit between intact and broken constraints for a relative radial motion between 2.5% and 3.2%. In the following, we keep the limit equal to 3% for all pairs of atoms, but we checked that small changes of the latter did not affect the constraint enumeration.

Note that this limit differs from the one obtained when averaging across all atoms. Indeed, in Figure 5, radial excursions are obtained by averaging both over time and over the atoms. Hence, large σ_r can arise either from a large atomic motion or from a structural disorder, with each atom showing a different average bond length. On the contrary, with this individual atom analysis, we access the intrinsic radial excursion of the neighbors. Therefore, this limit between intact and broken constraints is more fundamental, as it does not depend on the structural disorder.

The average numbers of BS constraints per species of atom that are obtained by this individual atom analysis are presented in Table 1. Note that each BS constraint is shared by an O atom

Table 1. Average Number of Bond-Stretching (BS) and Bond-Bending (BB) Constraints for Each Atomic Species in C−S−H[a]

atom	no. of BS constraints per atom	no. of BB constraints per atom	total
Si	4	5	7
Ca	4.8	0	4.8
H	1	0	1
BO		1	1
NBO_H		1	1
NBO_{Ca}		1	1

[a]For simplicity, all BS constraints are fully attributed to the cations.

and by a cation. However, for simplicity here, all BS constraints are arbitrarily fully attributed to the cations Si, Ca, and H. This allows the analysis of the environment for each species of O atom to be avoided. Obtained results for Si and H atoms are expected and consistent with the previous mean-field approach: Si atoms show 4 BS constraints with the O atoms of the tetrahedron, and H atoms show 1 BS constraint with the nearest O atom. On the other hand, Ca atoms show on average 4.8 active BS constraints with the surrounding oxygen atoms. This arises from the fact that each Ca atom is associated with a different number of BS constraints, between 4 (typically between the layers) and 6 (inside the layers). This legitimates this individual atom approach, as the mean-field approach cannot capture this heterogeneity. As observed for Na atoms,[35] this shows that the number of BS constraints created by an atom does not always follow the coordination number, so that one cannot rely on simple guesses to enumerate BS constraints.

4. BOND-BENDING CONSTRAINTS

We now focus on the enumeration of the BB constraints. To evaluate the angular excursion of each neighbor, we calculate the distribution of each angle formed around a central atom. We use the following convention: $i0j$ is the angle formed around the central atom 0 and by its neighbors i and j. If we restrict ourselves to the $N = 6$ nearest neighbors, then we get $N(N-1)/2 = 15$ different angles. A number is then attributed to each angle, following the ranking 102, 103, ..., 106, 203, ..., 506 (see the convention in the caption of Figure 7). Examples of such partial angular distributions, around Si atoms, are shown in Figure 7. The first moment of these distributions corresponds to the mean value of each angle, which is shown in

dx.doi.org/10.1021/jp502550z | J. Phys. Chem. C 2014, 118, 12485−12493

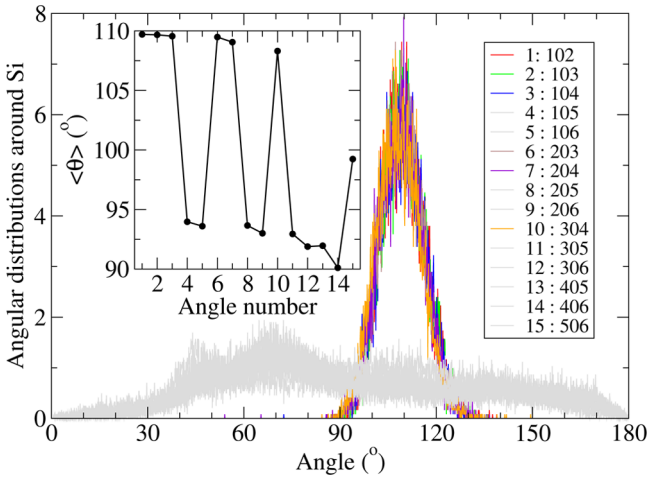

Figure 7. Angular distributions of every angle formed by Si atoms and their first six neighbors. The angle *i*0*j* corresponds to the angle formed by neighbors *i* and *j* and centered around the central Si atom 0. Sharp distributions (low angular excursion, intact bond-bending constraint) are colored, whereas flat distributions (large angular excursion, broken bond-bending constraint) are in gray. The inset shows the average value of each angle, following the indicated naming convention.

the inset of Figure 7 as a function of the angle number. Here, as expected, we recover that the four nearest O neighbors of each Si atom form a tetrahedron, with an average angle of 109°. A clear distinction is observed between the distributions of the angles involving the four nearest neighbors, which are sharp, and those involving further neighbors, which are much broader.

Following the same general method as presented for the BS constraints, the second moment of these distributions, the standard deviation σ_θ, gives an estimation of the angular excursion of each angle, i.e., the strength of the corresponding BB constraint. Once again, large σ_θ values correspond to broken constraints, whereas small ones arise from intact constraints. The σ_θ values are shown in Figure 8 around each atomic species. According to a previous study on the behavior of the constraints with temperature, the limit between intact and broken BB constraints was found to be around 14°.[35] However, one can observe that small changes of this limit do not involve any change in the results, as there is a clear gap between intact (low σ_θ) and broken (large σ_θ) BB constraints. Note that, as the average value of σ_θ of intact constraints is fairly similar around Si and O atoms (around 7°), there is no need here to rescale them with respect to the average bond angle.

In the case of Si atoms, we find six angles (102°, 103°, 104°, 203°, 204°, and 304°) showing a small σ_θ, around 6° (see Figure 8a). On the contrary, angles involving atoms of the second coordination shell around Si show a much larger σ_θ, around 35°. However, only five of these six angles are mutually independent, so that each Si atom experiences five BB constraints that define the tetrahedron. Once again, note that, in spite of the partial crystallinity of the silicate layers in C−S−H, we find no signature of BB constraints with neighbors outside the first coordination shell that would artificially result in some mutually dependent constraints. BO atoms show only one intact BB constraint that fixes the Si−BO−Si angle (see Figure 8b). NBO_{Ca} and NBO_H show the same behavior, with one intact BB constraint, which maintains the Si−NBO−X angle fixed around its average value, where X = Ca or H. This result differs from what has been observed in sodium silicate, in which NBO atoms do not show any angular constraint.[35] H and Ca cations significantly differ from Si and O atoms, as they do not show any BB constraint (see Figure 8c,d). Indeed, similarly to what was observed in the case of Na atoms,[35] Ca−O bonds show a more ionic character and are less directional than Si−O bonds, which are more covalent. We checked that these large σ_θ values do not arise from only an important structural disorder

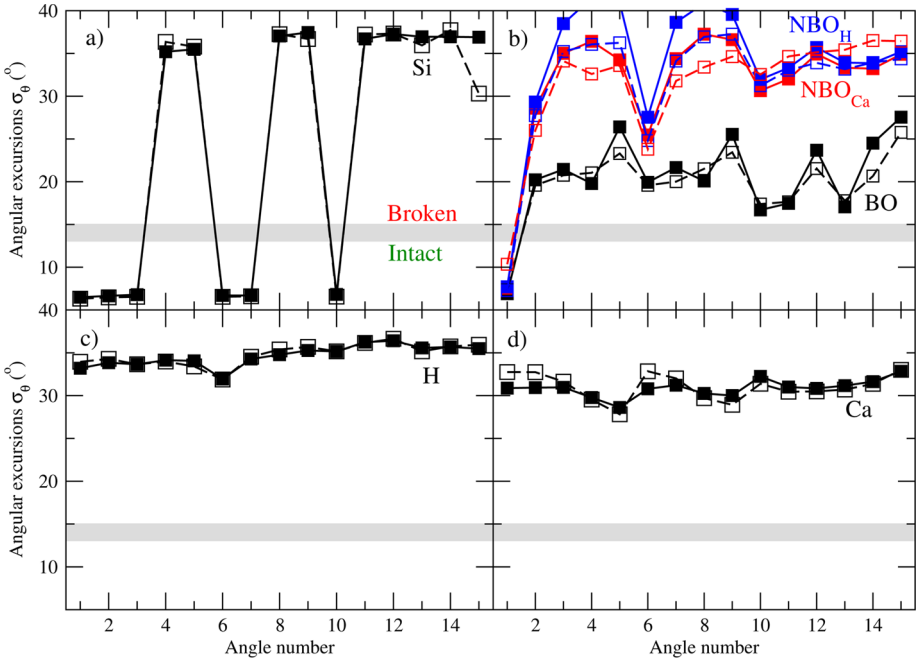

Figure 8. (a) Si, NBO_H, NBO_{Ca}, and BO, (c) H, and (d) Ca angular standard deviations σ_θ as a function of the angle number, where BO, NBO_H, and NBO_{Ca} correspond to bridging oxygen and nonbridging oxygen around H and Ca atoms, respectively. In all cases, the shaded area indicates an approximate limit between intact (low σ_θ) and broken (large σ_θ) bond-bending constraints.

dx.doi.org/10.1021/jp502550z | J. Phys. Chem. C 2014, 118, 12485−12493

by analyzing the angular distributions around each atom individually, in the same fashion as what has been presented in the case of the BS constraints. This enumeration is summarized in Table 1.

5. APPLICATION TO HARDNESS PREDICTION

The average numbers of BS and BB constraints associated with each species of atoms are given in Table 1. To determine the rigidity status of C−S−H, we calculate the number of constraints per atom from

$$n_c = \left(\sum_{i=1}^{N} x_i n_c^i\right) / \left(\sum_{i=1}^{N} x_i\right) \quad (3)$$

where N is the number of different atomic species, x_i is the atomic fraction of the ith species, and n_c^i is the average number of constraints (BS and BB) experienced by the ith species. Note that isolated molecules that are not part of the network, i.e., free hydroxyl groups and undissociated water molecules, are excluded from the enumeration, so the sum of the atomic fractions is lower than 1. However, we explicitly take into account terminal H atoms rather than considering a skeleton network, from which 1-fold atoms would have been removed. This form of enumeration has been shown to provide a better understanding of nanoindentation hardness values of hydrogenated diamond and silicon carbide networks.[50]

Here, we find that $n_c = 2.91$, so the considered model of C−S−H is flexible ($n_c < 3$). This means that the network shows some internal degrees of freedom, which can cause irreversible deformations and aging. As the hydration of C−S−H, which defines the number of H and NBO atoms that become part of the network, largely depends on the Ca/Si ratio,[24] it is mostly this latter ratio that controls the rigidity of the network. Indeed, let us consider the effect of replacing a SiO_2 group by a CaO group. SiO_2 shows 11 constraints shared by 3 atoms (see details in Table 2) and is, therefore, characterized by $n_c = 11/3 = 3.7$ (stressed rigid). On the contrary, CaO shows 4.4 constraints shared by 2 atoms (see details in Table 3), so $n_c = 2.2$ (flexible).

Table 2. Constraint Enumeration in a SiO_2 Group

atom	no.	no of BS constraints per atom	no. of BB constraints per atom	total
Si	1	4/2 = 2	5	9
O	2	2/2 = 1	1	2
total	3	4	7	11

Table 3. Constraint Enumeration in a CaO Group

atom	no.	no. of BS constraints per atom	no. of BB constraints per atom	total
Ca	1	4.8/2 = 2.4	0	2.4
O	1	2/2 = 1	1	2
total	2	3.4	1	4.4

Therefore, assuming that the average number of constraints created by each species of atom does not change significantly with composition, one can expect that decreasing the Ca/Si ratio would increase the rigidity of the network.

This is confirmed by performing the same rigidity analysis on C−S−H samples with different compositions. To understand the effect of the Ca/Si ratio on the rigidity of the network, we simulated two additional samples characterized by Ca/Si molar ratios of 1.09 and 1.33 following the same methodology. As shown in Figures 5 and 8, the radial and angular standard deviations around each atomic species weakly depend on the Ca/Si ratio. As such, the number of BS and BB constraints created by Si, Ca, H, and O atoms does not show significant changes with the composition. The inset of Figure 9 shows n_c for the three selected samples. As expected, n_c increases when the Ca/Si ratio decreases, reaching 3.46 for Ca/Si = 1.09. Hence, decreasing the amount of Ca allows the rigidity of the network to be increased, from a flexible ($n_c < 3$) to a stressed-rigid ($n_c > 3$) state.

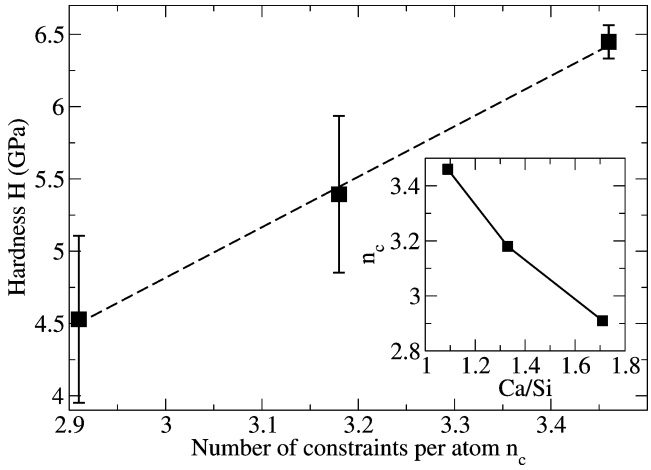

Figure 9. Computed hardness of C−S−H[21] with respect to the number of constraints per atom n_c. The dashed line is a linear fit. The inset shows n_c as a function of the Ca/Si molar ratio for the three selected samples.

Such an evolution of the number of constraints per atom with the composition is usual for network glasses, such as Ge−Se or As−Se chalcogenides.[40,43] As such, one can now apply to C−S−H all the theoretical tools developed in glass science, which link n_c to macroscopic properties. In particular, hardness, which characterizes the resistance to plastic deformations, was reported to increase linearly with n_c,[12] which allows prediction of the hardness H with respect to composition. As a preliminary study, we computed H for the three selected samples. The details of the calculation as well as experimental validations can be found in ref 21. As shown in Figure 9, H increases with the rigidity of the network, going from 4.5 GPa at Ca/Si = 1.71 to 6.4 GPa at Ca/Si = 1.09. Hence, it can be expected that the compositional dependence of the hardness of C−S−H could be predicted in the same fashion as for glasses.[12] This will be investigated in the future.

6. DISCUSSION

Finally, we aim at understanding the effect of hydration on the rigidity of the C−S−H network. To this end, we compare the present constraint enumeration with that of a calcium silicate glass, $(SiO_2)_{1-x}(CaO)_x$. To allow for a consistent comparison, we assume that the number of BS and BB constraints created by each atomic species is the same as in C−S−H. Note that the local environment of the glass might differ from that of C−S−H, especially for Ca atoms. Hence, this enumeration might not apply to a real calcium silicate glass. The details of the enumeration are presented in Table 4. For this system, the number of constraints per atom would be

dx.doi.org/10.1021/jp502550z | J. Phys. Chem. C 2014, 118, 12485−12493

Table 4. Constraint Enumeration for a Calcium Silicate System, $(SiO_2)_{1-x}(CaO)_x$, without Hydration[a]

atom	no.	no. of BS constraints per atom	no. of BB constraints per atom	total
Si	$1 - x$	4	5	7
Ca	x	4.8	0	4.8
O	$2 - x$		1	1
total	$3 - x$			$11 - 5.2x$

[a]For simplicity, all BS constraints are fully attributed to the cations.

$$n_c = \frac{11 - 5.2x}{3 - x} \tag{4}$$

The isostatic composition x_{iso} is obtained for $n_c = 3$:

$$\frac{11 - 5.2x_{iso}}{3 - x_{iso}} = 3 \tag{5}$$

Eventually, one gets $x_{iso} = 0.9$. This means that, for $x < 0.9$, dry calcium silicate would be stressed rigid and would be flexible for $x > 0.9$. For Ca/Si = 1.71, the composition of the studied C−S−H system, one would get $x = 0.63$, which falls into the stressed-rigid domain ($n_c = 3.3$). Therefore, without hydration, C−S−H with Ca/Si = 1.71 would be stressed rigid. This shows that the hydration plays a major role in the constraint enumeration. By depolymerizing the network with the creation of 1-fold-coordinated H atoms, the addition of water decreases the rigidity of the system. This is consistent with the experimental hardness values of hydrogenated diamond and silicon carbide networks,[50] which decrease with the degree of hydrogenation.

7. CONCLUSION

The use of realistic molecular dynamics simulations allows enumeration of the number of topological constraints in a molecular network without relying on simple guesses or unproven structural models. We have applied this method to study C−S−H, a complex and challenging material of great practical importance. It has been shown that the constraint enumeration algorithm can still be applied to partially crystalline systems. Moreover, by taking into account the existence of isolated molecules and of heterogeneities, we have extended the scope of rigidity theory. The results show that C−S−H with Ca/Si = 1.71, the average composition in ordinary Portland cement,[18] has a flexible network. This floppy character is mainly due to the hydration of the network. A detailed enumeration of the constraints for different compositions shows that decreasing the Ca/Si ratio improves the hardness of the material by increasing the number of constraints per atom, as observed for glasses. A careful tuning of the Ca/Si ratio would allow an optimally constrained isostatic C−S−H to be achieved, making it more likely to exhibit improved resistance to fracture and aging. In practice, a smaller Ca/Si ratio can be obtained by adding silica fume or fly ash to the cementitious constituents. We note that decreasing the amount of calcium in cement would also lead to greener cement, as the preparation of the calcium oxides used for the clinker is the primary cause of carbon dioxide emissions during cement production, contributing 7% to total global CO_2 emissions.[51] More generally, this suggests that rigidity theory can be applied to the study and optimization of a broad range of complex materials of industrial importance.

AUTHOR INFORMATION

Corresponding Author

*E-mail: bauchy@mit.edu.

Notes

The authors declare no competing financial interest.

ACKNOWLEDGMENTS

This work has been carried out within the framework of the ICoME2 Labex (Grant ANR-11-LABX-0053) and the A*MIDEX projects (Grant ANR-11-IDEX-0001-02) cofunded by the French program Investissements d'Avenir, which is managed by the ANR, the French National Research Agency.

REFERENCES

(1) Phillips, J. C. Topology of covalent non-crystalline solids 0.1. Short-range order in chalcogenide alloys. *J. Non-Cryst. Solids* **1979**, *34*, 153−181.

(2) Phillips, J. C. Topology of covalent non-crystalline solids II: Medium-range order in chalcogenide alloys and As-Si-Ge. *J. Non-Cryst. Solids* **1981**, *43*, 37−77.

(3) Thorpe, M. F. Continuous deformations in random networks. *J. Non-Cryst. Solids* **1983**, *57*, 355−370.

(4) Mauro, J. C. Topological constraint theory of glass. *Am. Ceram. Soc. Bull.* **2011**, *90*, 31−37.

(5) Lagrange, J. *Mécanique Analytique*; Gauthier-Villars: Paris, 1788. Maxwell, J. C. *Philos. Mag.* **1864**, *27*, 294.

(6) Naumis, G. G. Energy landscape and rigidity. *Phys. Rev. E* **2005**, *71*, 026114.

(7) Feng, X.; Bresser, W. J.; Boolchand, P. Direct Evidence for Stiffness Threshold in Chalcogenide Glasses. *Phys. Rev. Lett.* **1997**, *78*, 4422−4425.

(8) Chubynsky, M. V.; Briere, M. A.; Mousseau, N. Self-organization with equilibration: A model for the intermediate phase in rigidity percolation. *Phys. Rev. E* **2006**, *74*.

(9) Rompicharla, K.; Novita, D. I.; Chen, P.; Boolchand, P.; Micoulaut, M.; Huff, W. Abrupt boundaries of intermediate phases and space filling in oxide glasses. *J. Phys.: Condens. Matter* **2008**, *20*, No. 202101.

(10) Chakravarty, S.; Georgiev, D. G.; Boolchand, P.; Micoulaut, M. Ageing, fragility and the reversibility window in bulk alloy glasses. *J. Phys.: Condens. Matter* **2005**, *17*, L1.

(11) Guin, J.-P.; Rouxel, T.; Sanglebœuf, J.-C.; Melscoët, I.; Lucas, J. Hardness, Toughness, And Scratchability of Germanium−Selenium Chalcogenide Glasses. *J. Am. Ceram. Soc.* **2002**, *85*, 1545−1552.

(12) Smedskjaer, M. M.; Mauro, J. C.; Yue, Y. Prediction of Glass Hardness Using Temperature-Dependent Constraint Theory. *Phys. Rev. Lett.* **2010**, *105*, 115503.

(13) Smedskjaer, M. M.; Mauro, J. C.; Sen, S.; Deubener, J.; Yue, Y. Impact of network topology on cationic diffusion and hardness of borate glass surfaces. *J. Chem. Phys.* **2010**, *133*.

(14) Mauro, J. C.; Ellison, A. J.; Pye, L. D. Glass: the Nanotechnology Connection. *Int. J. Appl. Glass Sci.* **2013**, *4*, 64−75.

(15) Mauro, J. C.; Smedskjaer, M. M. Unified physics of stretched exponential relaxation and Weibull fracture statistics. *Phys. A (Amsterdam, Neth.)* **2012**, *391*, 6121−6127.

(16) Rader, A. J.; Hespenheide, B. M.; Kuhn, L. A.; Thorpe, M. F. Protein unfolding: Rigidity lost. *Proc. Natl. Acad. Sci. U.S.A.* **2002**, *99*, 3540−3545.

(17) Phillips, J. C. Constraint theory and hierarchical protein dynamics. *J. Phys.: Condens. Matter* **2004**, *16*, S5065−S5072.

(18) Allen, A. J.; Thomas, J. J.; Jennings, H. M. Composition and density of nanoscale calcium−silicate−hydrate in cement. *Nat. Mater.* **2007**, *6*, 311−316.

(19) Pellenq, R. J.-M.; Kushima, A.; Shahsavari, R.; Vliet, K. J. V.; Buehler, M. J.; Yip, S.; Ulm, F.-J. A realistic molecular model of cement hydrates. *Proc. Natl. Acad. Sci. U.S.A.* **2009**, *106*, 16102−16107.

(20) Manzano, H.; Moeini, S.; Marinelli, F.; van Duin, A. C. T.; Ulm, F.-J.; Pellenq, R. J.-M. Confined Water Dissociation in Microporous Defective Silicates: Mechanism, Dipole Distribution, and Impact on Substrate Properties. *J. Am. Chem. Soc.* **2012**, *134*, 2208−2215.
(21) Abdolhosseini Qomi, M.; Krakowiak, K.; Bauchy, M.; Stewart, K.; Shahsavari, R.; Jagannathan, D.; Brommer, D.; Baronnet, A.; Buehler, M.; Van Vliet, K.; Yip, S.; Ulm, F.-J.; Pellenq, R. J.-M. Concrete under the nanoscope: Combinatorial optimization by screening defect attributes. *Nat. Commun.*, submitted for publication.
(22) Abdolhosseini Qomi, M.; Bauchy, M.; Pellenq, R. J.-M.; Ulm, F.-J. Applying Tools from Glass Science to Study Calcium-Silicate-Hydrates. *Mechanics and Physics of Creep, Shrinkage, and Durability of Concrete*, Proceedings of the Ninth International Conference on Creep, Shrinkage, and Durability Mechanics (CONCREEP-9), Cambridge, MA, Sept 22−25, 2013; American Society of Civil Engineers: Reston, VA, 2013; pp 78−85.
(23) Bauchy, M.; Abdolhosseini Qomi, M. J.; Pellenq, R. J.-M.; Ulm, F.-J. Order and Disorder in Calcium−Silicate−Hydrate *J. Chem. Phys.*, submitted for publication.
(24) Qomi, M. J. A.; Bauchy, M.; Ulm, F.-J.; Pellenq, R. J.-M. Anomalous composition-dependent dynamics of nanoconfined water in the interlayer of disordered calcium-silicates. *J. Chem. Phys.* **2014**, *140*, 054515.
(25) Soyer-Uzun, S.; Chae, S. R.; Benmore, C. J.; Wenk, H.-R.; Monteiro, P. J. M. Compositional Evolution of Calcium Silicate Hydrate (C−S−H) Structures by Total X-Ray Scattering. *J. Am. Ceram. Soc.* **2012**, *95*, 793−798.
(26) Hamid, S. The Crystal-Structure of the 11-A Natural Tobermorite $Ca_{2.25}[Si_3O_{7.5}(OH)_{1.5}]\cdot 1H_2O$. *Z. Kristallogr.* **1981**, *154*, 189−198.
(27) Abdolhosseini Qomi, M.; Ulm, F.-J.; Pellenq, R. J.-M. Evidence on the Dual Nature of Aluminum in the Calcium-Silicate-Hydrates Based on Atomistic Simulations. *J. Am. Ceram. Soc.* **2012**, *95*, 1128−1137.
(28) Plimpton, S. Fast parallel algorithms for short-range molecular dynamics. *J. Comput. Phys.* **1995**, *117*, 1−19.
(29) Bauchy, M. Structural, vibrational, and elastic properties of a calcium aluminosilicate glass from molecular dynamics simulations: The role of the potential. *arXiv.org, e-Print Arch., Condens. Matter* **2014**, No. 1403.1640.
(30) Wright, A. C. The comparison of molecular dynamics simulations with diffraction experiments. *J. Non-Cryst. Solids* **1993**, *159*, 264−268.
(31) Skinner, L. B.; Chae, S. R.; Benmore, C. J.; Wenk, H. R.; Monteiro, P. J. M. Nanostructure of Calcium Silicate Hydrates in Cements. *Phys. Rev. Lett.* **2010**, *104*, 195502.
(32) Meral, C.; Benmore, C. J.; Monteiro, P. J. M. The study of disorder and nanocrystallinity in C−S−H, supplementary cementitious materials and geopolymers using pair distribution function analysis. *Cem. Concr. Res.* **2011**, *41*, 696−710.
(33) Bauchy, M. Structural, vibrational, and thermal properties of densified silicates: Insights from molecular dynamics. *J. Chem. Phys.* **2012**, *137*, 044510.
(34) Bauchy, M.; Qomi, M. A.; Pellenq, R. J. M.; Ulm, F. J. Is cement a glassy material? *Comput. Modell. Concr. Struct.* **2014**, 169.
(35) Bauchy, M.; Micoulaut, M. Atomic scale foundation of temperature-dependent bonding constraints in network glasses and liquids. *J. Non-Cryst. Solids* **2011**, *357*, 2530−2537.
(36) Ganster, P.; Benoit, M.; Kob, W.; Delaye, J.-M. Structural properties of a calcium aluminosilicate glass from molecular-dynamics simulations: A finite size effects study. *J. Chem. Phys.* **2004**, *120*, 10172−10181.
(37) Gupta, P. K.; Mauro, J. C. Composition dependence of glass transition temperature and fragility. I. A topological model incorporating temperature-dependent constraints. *J. Chem. Phys.* **2009**, *130*, 094503−094503-8.
(38) Mauro, J. C.; Gupta, P. K.; Loucks, R. J. Composition dependence of glass transition temperature and fragility. II. A topological model of alkali borate liquids. *J. Chem. Phys.* **2009**, *130*, 234503−234503-8.
(39) Micoulaut, M.; Raty, J.; Otjacques, C.; Bichara, C. Understanding amorphous phase-change materials from the viewpoint of Maxwell rigidity. *Phys. Rev. B* **2010**, *81*.
(40) Bauchy, M.; Micoulaut, M.; Celino, M.; Le Roux, S.; Boero, M.; Massobrio, C. Angular rigidity in tetrahedral network glasses with changing composition. *Phys. Rev. B* **2011**, *84*, 054201.
(41) Bauchy, M. Topological constraints and rigidity of network glasses from molecular dynamics simulations. *Am. Ceram. Soc. Bull.* **2012**, *91*, 34−38A.
(42) Micoulaut, M.; Bauchy, M. Anomalies of the first sharp diffraction peak in network glasses: Evidence for correlations with dynamic and rigidity properties. *Phys. Status Solidi B* **2013**, *250*, 976−982.
(43) Bauchy, M.; Micoulaut, M.; Boero, M.; Massobrio, C. Compositional Thresholds and Anomalies in Connection with Stiffness Transitions in Network Glasses. *Phys. Rev. Lett.* **2013**, *110*, 165501.
(44) Bauchy, M.; Micoulaut, M. Transport Anomalies and Adaptative Pressure-Dependent Topological Constraints in Tetrahedral Liquids: Evidence for a Reversibility Window Analogue. *Phys. Rev. Lett.* **2013**, *110*, 095501.
(45) Bauchy, M.; Micoulaut, M. Structure of As2Se3 and AsSe network glasses: Evidence for coordination defects and homopolar bonding. *J. Non-Cryst. Solids* **2013**, *377*, 34−38.
(46) Bauchy, M. Structure and dynamics of liquid $AsSe_4$ from ab initio molecular dynamics simulation. *J. Non-Cryst. Solids* **2013**, *377*, 39−42.
(47) Bauchy, M.; Micoulaut, M. Percolative heterogeneous topological constraints and fragility in glass-forming liquids. *EPL* **2013**, *104*, 56002.
(48) Micoulaut, M.; Kachmar, A.; Bauchy, M.; Le Roux, S.; Massobrio, C.; Boero, M. Structure, topology, rings, and vibrational and electronic properties of Ge_xSe_{1-x} glasses across the rigidity transition: A numerical study. *Phys. Rev. B* **2013**, *88*, 054203.
(49) Lindemann, F. A. Ueber die berechnung molekularer eigenfrequenzen. *Phys. Z.* **1910**, *11*, 609−612.
(50) Boolchand, P.; Zhang, M.; Goodman, B. Influence of one-fold-coordinated atoms on mechanical properties of covalent networks. *Phys. Rev. B* **1996**, *53*, 11488−11494.
(51) Mehta, P. K. Reducing the environmental impact of concrete. *Concr. Int.* **2001**, *23*, 61−66.